Effects of torsion on the thermal conductivity of multi-layer graphene

Chao Si,[1,2] Gui Lu,[1,2] Bing-Yang Cao,[3,a)] Xiao-Dong Wang,[1,2,a)] Zhen Fan,[4] and Zhi-Hai Feng[4]

[1]*Research Center of Engineering Thermophysics, North China Electric Power University, Beijing 102206, China*
[2]*School of Energy Power and Mechanical Engineering, North China Electric Power University, Beijing 102206, China*
[3]*Key Laboratory for Thermal Science and Power Engineering of Ministry of Education, Department of Engineering Mechanics, Tsinghua University, Beijing 100084, China*
[4]*Key Laboratory of Advanced Functional Composite Materials, Aerospace Research Institute of Materials and Processing Technology, Beijing 100076, China*

(Received 18 February 2017; accepted 8 May 2017; published online 22 May 2017)

This work employs the equilibrium molecular dynamics method to study the effects of torsion on the thermal conductivity of multi-layer graphene. Thermal conductivities of twisted 10-layer 433.91×99.68 Å^2 graphene with torsion angles of 0°, 11.25°, 22.5°, 33.75°, 45°, 67.5°, 90°, 112.5°, and 135° are calculated. The corresponding radial distribution functions and nearest atomic distances are calculated to reveal the effects of torsion on lattice structures. The spectral energy density (SED) method is utilized to analyze the phonon transport properties. It is very interesting that the thermal conductivity of multi-layer graphene decreases slightly at first and then increases with the increasing torsion angle, and the valley is located at $\theta_G = 22.5°$ with the lowest thermal conductivity of 4692.40 W m^{-1} K^{-1}. The torsion effect can be considered as a combination of the compression effect and the dislocation effect. Further SED analysis confirms that the effect of dislocation on thermal conductivities can be negligible, while the compression effect decreases the phonon lifetimes of flexural out-of-plane acoustic (ZA) branches and increases the ZA group velocities and the phonon specific heat. The decrease becomes dominated when the torsion angle is small, whereas the increase becomes more and more dominated when the torsion angle becomes larger, which are responsible for the reported variation of thermal conductivities. *Published by AIP Publishing*. [http://dx.doi.org/10.1063/1.4983812]

I. INTRODUCTION

As a two-dimensional (2D) material formed by hexagonally arranged carbon atoms, graphene has attracted significant attention in the thermal management field of the composite and semiconductor industry due to its ultrahigh thermal conductivity. Various studies including experiments,[1,2] theoretical calculations,[3,4] and modeling predictions[5,6] have been carried out to reveal the thermal properties of graphene and the influences of substrates, defects, and other atomic modifications, which were comprehensively reviewed in Refs. 7 and 8. In the industrial production process of graphene, it has been found that multi-layer graphene (MLG) is easily fabricated and has a higher electrical controllability than monolayer graphene.[9] Therefore, MLG and its derivatives, including graphene-based membranes[10] and graphite nano-platelet/nano-sheets,[11,12] are of economic benefit and have been cosmically produced in industry. The graphene-based membrane has the MLG structure with 1–100 layers and macro-scale in-plane sizes[10] and has been widely used in integrated circuits, touch screens, and semiconductor industry. In the applications of graphene-based membranes, high electric conductivity and low thermal conductivity are required. On the other hand, as an important matrix material in thermal conductive composites, graphite nano-platelet/nano-sheet has the MLG structure with ~30 layers and in-plane sizes of 1–100 μm,[11–13] where the high thermal conductivity is needed. Thus, there is a demand for quantitatively tuning the thermal conductivity in the applications of MLG.

Since the interlayer atomic interactions in MLG introduce extra phonon-phonon scattering in the material, the thermal transport in MLG is more complex than that in monolayer graphene. Lindsay and his co-workers[14] summarized that there exist three unknown key points about the thermal transport in MLG. The first point is the effect of the layer number on the in-plane thermal conductivity of MLG and its mechanism. The second point is the extent of the diffusive transport regime of the phonon. The third point is the stress effect on the intrinsic in-plane thermal conductivity. In fact, stress can continuously manipulate the thermal transport properties of materials, which is easy to perform even at the nano-scale.[15] Recently, the stress effects on the thermal conductivity of monolayer graphene have been reported by several researches. Li *et al.*[16] found that the additional tensile/compressive stresses affect the mode-specific group velocities and the specific heat in monolayer graphene, and there exists a peak value of thermal conductivity when tuning the stress from the compression to the strain. Wei *et al.*[15] exerted combinational strains on a monolayer graphene sheet in both directions parallel and perpendicular to the thermal transfer

a)Authors to whom correspondence should be addressed: wangxd99@gmail.com, Tel./Fax: +86-10-62321277 and caoby@tsinghua.edu.cn, Tel./Fax: +86-10-62794531.

path and concluded complex effects on thermal conductivities. Some of the graphene under complex strain can have higher thermal conductivity than that of a free-standing graphene without strain. In a word, their studies have provided a deep understanding of the mechanism of stress effects.

In contrast to monolayer graphene, MLG has a quasi-2D structure with weak coupling between layers. MLG somewhat exhibits the thermal properties of the bulk materials, especially when the layer number is larger than 5. Specifically, the cross-plane thermal conductivity,[17] in-plane thermal conductivity,[18] and the evolution of the strain effect on in-plane thermal conductivity[14] are all closer to those properties of bulk graphite for MLG that the layer number is much larger than 5. Meanwhile, several 2D characteristics are still not reported. Lindsay's group[14] found that the thermal conductivity of MLG first increases and then decreases along with the increasing strain where the largest enhancement amplitude is about 40%. The competition between the decreased phonon heat capacities and the increased lifetimes of flexural phonons with increasing strain contributes to this behavior. In fact, the decreased phonon specific heat can be regarded as the characteristic of the bulk material, while the increased lifetimes of flexural phonons can be regarded as the characteristic of the 2D material. It is reasonable that more complex thermal properties can be found for MLG as a classical quasi-2D material.

The effect of the torsion stress on the thermal conductivity of graphene is still an open question, even if the torsion stress has been a common kind of stresses in the applications of materials. As shown in Table I, several literatures have observed that the acoustic phonon scattering is aggravated when a monolayer graphene is twisted, which decreases the thermal conductivities.[15,19–22] However, Refs. 15, 19, 21, and 22 did not report on the quantitative analysis about phonon scattering. Additionally, in Ref. 20, the effect of the torsion stress on (1–3)-layer graphene with zigzag chirality was further studied, where the Green function was utilized to calculate the phonon dispersion curves. It was observed that the flexural out-of-plane acoustic (ZA), transverse acoustic (TA), and longitudinal acoustic (LA) phonon modes become slightly soften as the torsion stress is applied, and thus, the thermal conductivities decrease. Moreover, the trend of the decreasing thermal conductivities slows down when the layer number increases from 1 to 3, which has not been explained in Ref. 20. Unfortunately, Ref. 20 did not present any important details on how the phonon dispersion curves were calculated by the Green function. In twisted graphene, it is difficult to define a unit cell, in contrast to that in the flat graphene. It is worth noting that the width of graphene applied in Ref. 20 is only 1 nm, which inevitably introduces very strong phonon boundary scattering into the system. The softening of acoustic phonon modes may be related to the boundary scattering. By reviewing the previous literatures, it is concluded that further research is needed to reveal the mechanism of torsion effects on thermal conductivities of MLG.

TABLE I. Previous literature about the torsion effects on thermal conductivities of graphene.

References	Chirality of graphene	Size (nm^2)	Torsion angle
15	Zigzag	2.1×10	$0, \pi, 2\pi, 3\pi$
19	Zigzag	10.4×100	1°–10°
20	Zigzag	1×80 (1–3 layers)	$0, 2\pi, 4\pi, 6\pi, 8\pi, 10\pi$
21	Armchair/Zigzag	1.4×15.8	$0, \pi, 2\pi, 3\pi, 4\pi$
22	Zigzag	(44.28–103.3) × (59.64–187.44)	0, 60°, 120°, 180°, 240°, 300°, 305°

Due to the atom-scale thickness, the measurement of the thermal conductivity of graphene is challenging. Several experimental studies[1,2,23–25] have been carried out to measure the thermal conductivity of graphene, but the measured values are strongly affected by the sample quality, sample size, and experimental strategy. As a result, the numerical simulation methods[19–23,26–32] have been become important tools for further understanding of the thermal properties such as Molecular dynamics (MD) simulations,[19–23] Boltzmann transport equation (BTE) simulations,[27–29] and non-equilibrium Green's functions (NEGF) simulations.[30–32] The MD simulation method employs atomic interactions as a force field and atomic motions can be followed by solving the classic Newtonian equations. It has been found that there is some discrepancy with BTE studies and NEGF approaches in the prediction of thermal conductivity, but the m-phonon process for $m > 3$ can be modeled reasonably in MD simulations. Thus, MD simulations have been extensively used to analyze the effects of atomistic changes on the thermal properties of a nanomaterial, as the quantum correction[33] is involved.

Technically, it is very hard to obtain the phonon spectrum of the twisted MLG structure directly in MD simulations, where the main difficulty is defining the unit cells of the structure and the failure of the periodical boundary condition. Another problem is that calculating the phonon spectrum of the whole twisted structure requires huge computational capacity. In fact, even for the flat graphene, it has been revealed that computational capacity is the bottleneck when calculating the phonon spectrum. Wei *et al.*[34] have estimated that, to obtain the phonon spectrum of the graphene with 2400 carbon atoms, the amount of data produced by a normal simulation of 4 ns reaches up to 50 Gb. To solve the problem, we raise a new equivalent method to analyze the torsion effects on the phonon spectrum of MLG. As a brief introduction, the equilibrium molecular dynamics (EMD) method will be utilized to present the effects of torsion on thermal conductivities of MLG; meanwhile, the torsion effects on the lattice constant and nano-structure will be quantitatively discussed to reveal the mechanism.

II. MODELS AND SIMULATION DETAILS

The EMD simulation method is utilized to study the effects of torsion on thermal conductivities of multi-layer graphene. The snapshots for the 10-layer graphene with torsion angles of 0°, 22.5°, 45°, 67.5°, 90°, 112.5°, and 135° are shown in Fig. 1. The coordinate axes and the origin are defined as those in Fig. 1(a). It has been tested that the structure will be destroyed if the torsion angle is larger than 135°. For the original graphene without torsion [Fig. 1(a)], the in-plane size is 433.91×99.68 Å^2, the chirality in the x-direction is armchair, and the interlayer distance of the

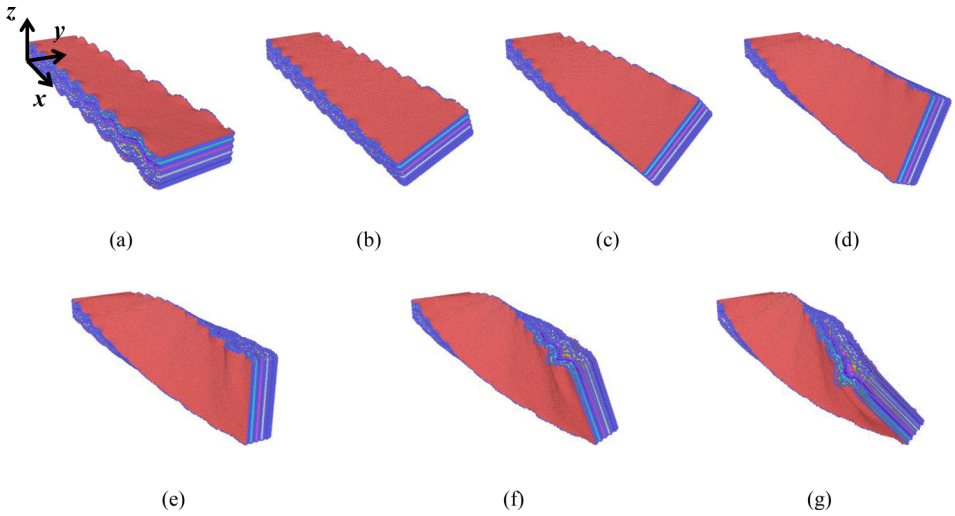

FIG. 1. Schematic diagrams of the twisted 10-layer 433.91 × 99.68 Å^2 graphene, whose torsion angles are (a) 0°, (b) 22.5°, (c) 45°, (d) 67.5°, (e) 90°, (f) 112.5°, and (g) 135°, respectively.

graphene is 3.4 Å. The torsional strain is achieved by creating an initially twisted structure through Eqs. (1)–(4). The Polak-Ribiere algorithm[35] is adopted to optimize the structure

$$\theta_i(x_i) = x_i \times \frac{\theta_G}{L_G}, \tag{1}$$

$$x_i = x_{i,0}, \tag{2}$$

$$y_i = (y_{i,0} - y_m) \times \cos\theta_i + y_m, \tag{3}$$

$$z_i = (z_{i,0} - z_m) \times \sin\theta_i + z_m, \tag{4}$$

where x_i, y_i, and z_i are the coordinates of the ith atom at x-, y-, and z-axes after the torsion, $x_{i,0}$, $y_{i,0}$, and $z_{i,0}$ are the coordinates before the torsion, $L_G = 433.91$ Å is the length of the graphene, θ_G is the torsion angle, θ_i is the local torsion angle for the ith atom, y_m and z_m denote the location of the yz-plane center, $y_m = 49.84$ Å, and $z_m = 17.00$ Å. Thus, the torsion axis locates at the center of the yz-plane and parallel to the x-direction.

The opt-Tersoff[36] many-body potential model is used to model the intralayer atomic interactions in the graphene. To reduce the edge scattering, the carbon atoms on the edges are saturated by hydrogen atoms. The carbon-hydrogen interactions are simplified into the harmonic effect. The 12-6 Lennard-Jones potential model is used to simulate the interlayer interactions, as described in the following equation:

$$V_{ij}^{LJ} = 4\varepsilon_{ij}\left[\left(\frac{\sigma_{ij}}{r_{ij}}\right)^{12} - \left(\frac{\sigma_{ij}}{r_{ij}}\right)^{6}\right], \tag{5}$$

where V_{ij}^{LJ} is the potential between atoms i and j, r_{ij} is the distance between i and j, and σ_{ij} and ε_{ij} denote the minimum energy and the zero energy separation distance ($\sigma_{ij} = 3.4$ Å and $\varepsilon_{ij} = 0.00251$ eV). The LAMMPS package[37] is used to carry out the EMD simulation. The velocity-Verlet algorithm is utilized. The time step is set as 0.001 ps. The size of the simulation box is $500 \times 150 \times 150$ Å^3, which is large enough for the torsional graphene whose initial size is $433.91 \times 99.68 \times 34$ Å^3. The graphene is located in the center of the simulation box. The relaxation equilibrium state of the graphene can be obtained by performing the isothermal-isobaric (NPT) simulation at 300 K, 0 Pa for 300 ps, followed by microcanonical (NVE) simulation for 600 ps. During the relaxation, the two ends of the torsional graphene are kept fixed in all directions, and hence, the graphene length remains at a constant value of 433.91 Å. It should be noted that there exists a drop of the total internal energy of the graphene from the NPT approach to the NVE approach, due to the release of the inner stress which is blocked in the unfixed region during the NPT simulation process.

To calculate the thermal conductivities of the torsional graphene, the Green-Kubo[38] theory is utilized in the following NVE simulation for 2 ns, as described in the following equation:

$$\lambda_x = \frac{V}{k_B T^2}\int_0^\infty \langle J_x(0) J_x(t)\rangle \mathrm{d}t, \tag{6}$$

where λ_x denotes the thermal conductivity in the x-direction, $J_x(t)$ denotes the heat flux at time t in the x-direction, V is the volume of MLG, k_B is the Boltzmann constant, T is the temperature, and $\langle\ \rangle$ denotes the ensemble average. For the twisted MLG, the volume of the initial structure defined by Eqs. (1)–(4) can be easily calculated by geometric relationships between Eqs. (3) and (4). However, after the relaxation equilibrium process, the interlayer bonding force starts to work and the structure is tensioned, which may decrease the volume of MLG. Thus, $V = R_d V_{initial}$, $0 < R_d < 1$, where R_d denotes the deformation rate which can be estimated by dividing the average interlayer distance of twisted MLG by that of flat MLG without torsion. Since the intralayer carbon-carbon atomic interactions are simulated by the opt-Tersoff many-body potential model,[36] Eq. (7) raised by Li *et al.*[39] is adopted to calculate the heat flux term in Eq. (6) as follows:

$$\mathbf{J} = \frac{1}{V}\left(\sum_{i=1}^{n}\vec{v}_i\delta_i + \frac{1}{2}\vec{r}_{ij}\left(\Delta\vec{F}_j\cdot\vec{v}_j - \Delta\vec{F}_i\cdot\vec{v}_i\right) - \frac{1}{2}\left(\vec{r}_{jk} - \vec{r}_{ki}\right)\left(\Delta\vec{F}_k\cdot\vec{v}_k\right)\right), \tag{7}$$

where $\mathbf{J} = (J_x, J_y, J_z)$ is the heat flux vector, $\vec{v}_i$ is the velocity vector of atom i, δ_i is the internal energy of atom i, $\vec{r}_{ij} = \vec{r}_i - \vec{r}_j$ is the distance vector from atoms i to j, and $\Delta\vec{F}_i$ is

the contribution of atom i to the many-body potential W_{ijk}^{Tersoff}, which denotes the potential value between atoms i, j, and k. $\Delta\vec{F}_\alpha = -\partial W_{ijk}^{\text{Tersoff}}/\partial\vec{r}_\alpha$, where $\alpha = i, j$, and k.

Since there are statistical errors for the auto-correlation function terms with different time-steps in Eq. (6), the phase space average method[40] is adopted, where the average indexes $N_{\text{every}} = 10$, $N_{\text{repeat}} = 200$, and $N_{\text{freq}} = 2000$; here, N_{every} denotes the number of the time-steps that needed to input values, N_{repeat} denotes the number of correlation time windows to accumulate, and N_{freq} denotes the number of the time-steps that needed to calculate the time window averages. Moreover, in MD simulations, the quantum effects cannot be considered so that the quantum correction[33] is utilized in this work since Debye temperature for graphene is much larger than 300 K.[7] The correction factor utilized in this work is $dT_{\text{MD}}/dT = 0.851$, which is the same as that in Ref. 33.

The phonon relaxation time and axial phonon group velocity can be calculated by the spectral energy density (SED) method, which is raised by McGaughey's group.[41] The SED represents the average kinetic energy per unit cell. SED formula Φ can be expressed as a function of the wave-vector in the βth direction $\mathbf{q}_\beta$ and the frequency ω, or

$$\Phi(\mathbf{q}_\beta,\omega) = \frac{1}{4\pi\tau_0 l}\sum_{\alpha,b} m_b \left\| \int_0^{\tau_0} \sum_l \dot{u}_\alpha(l,b) \times \exp\left(i\mathbf{q}_\beta \cdot \mathbf{r}(l,0) - i\omega t\right) dt \right\|^2, \quad (8)$$

where m_b is the mass of atom b, l is the total number of the primitive cell, τ_0 is the SED calculation time, $\dot{u}_\alpha(l,b)$ are the velocities of atom b in the α direction inside the lth cell, $\mathbf{r}(l,0)$ is the equilibrium position vector of the lth cell, and i is the imaginary unit. The polarization information can be identified by dividing Φ into one out-of-plane direction and two in-plane directions. The region that contains the specified peak is chosen to fit the peak frequency by the following Lorentzian function:

$$\Phi(\mathbf{q}_\beta,\omega) = \frac{I}{1+\left[(\omega-\omega_c)/\gamma\right]^2}, \quad (9)$$

where I is the peak magnitude, ω_c is the frequency at the peak center, and γ is the half-width at half-maximum. Thus, the phonon lifetime can be defined as $\tau = 1/2\gamma$, and the axial phonon group velocity can be defined as $v_{g,\beta} = \partial\omega/\partial\mathbf{q}_\beta$.

III. RESULTS AND DISCUSSION

The effects of the torsion angle on the thermal conductivities and the lattice characteristics of the 10-layer graphene are studied. The structure of multilayer graphene is anisotropic so that the interlayer and intralayer atomic structures and interactions will be discussed separately. Since it is difficult for the SED method to calculate the phonon dispersion of the torsional structure, an equivalent approach is proposed to analyze the phonon dispersion. Section III A shows the thermal conductivities calculated by the Green-Kubo[38] theory, Section III B shows the effects of torsion on lattice structures, and Section III C shows the phonon dispersion analysis.

A. Thermal conductivity

The EMD approach is utilized to predict the thermal conductivity of the twisted MLG, where four individual Green-Kubo[38] thermal conductivities are calculated for each structure as repeated tests. As shown in Fig. 2(a), the time evolutions of the four calculated thermal conductivities (the gray lines) and their averaging value (the red line) for the MLG with $\theta_G = 0°$ are presented. Due to the noise problem for term $\langle J_x(0)J_x(t)\rangle$ in the x-direction, there exists disagreement among the four calculated thermal conductivities. Since the linear response process cannot reach the steady state until $t > 500$ ps, the calculated values for 1200 ps $< t <$ 1500 ps are adopted based on the derivation in Ref. 42. For MLG with $\theta_G = 0°$, the predicted thermal conductivity of 5080 W m^{-1}K^{-1} is obtained, whose positive error is 377.6 W m^{-1}K^{-1} and negative error is −318.4 W m^{-1}K^{-1} based on the values of the test cases at 1250 ps $< t <$ 1500 ps. In the previous work by Lindsay's group[3], the BTE method is utilized to indicate that the thermal conductivity of single-layer graphene is about 3500 W m^{-1}K^{-1}. It has been widely found that there is some discrepancy between

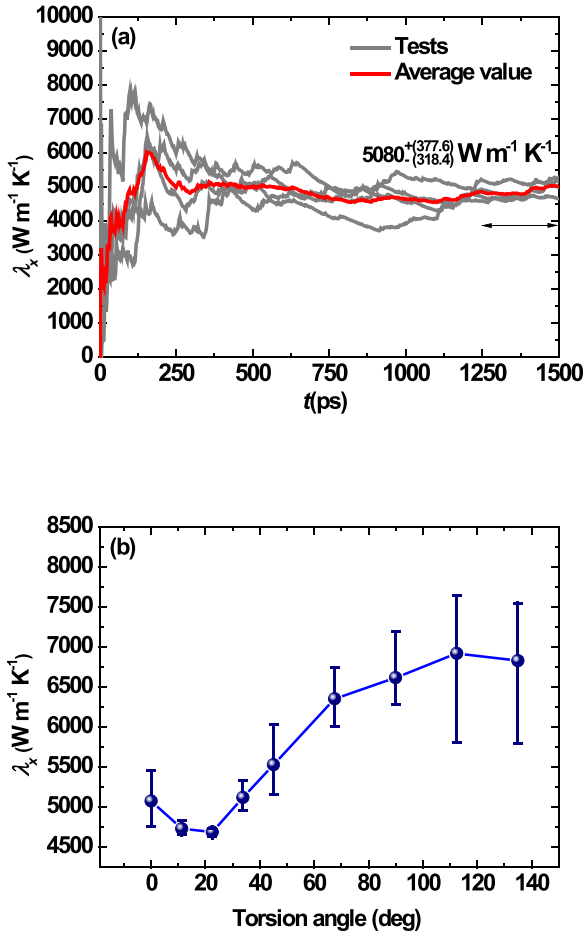

FIG. 2. (a) Time evolutions of the four calculated thermal conductivities (the gray lines) and their average value (the red line) for MLG with $\theta_G = 0°$. (b) Thermal conductivities predicted by EMD simulations of twisted MLG with $\theta_G = 0°$, 11.25°, 22.5°, 33.75°, 45°, 67.5°, 90°, 112.5°, and 135°.

the BTE method and MD simulations. For the BTE method, m-phonon processes for all the m that is $m > 3$ cannot be modeled overall. Thus, the discrepancy between the BTE method and MD simulations can be attributed to different physical assumptions of the two methods. Similarly, the thermal conductivities of twisted MLG with $\theta_G = 0°$, 22.5°, 45°, 67.5°, 90°, 112.5°, and 135° can be predicted in EMD simulations, as shown in Fig. 2(b). The thermal conductivity decreases slightly first and then increases with the increasing torsion angle, and the valley is located at $\theta_G = 22.5°$ with the lowest thermal conductivity of 4692.40 W m^{-1} K^{-1}. Two extra cases of $\theta_G = 11.25°$ and $\theta_G = 33.75°$ are added to Fig. 2(b) to make the valley more distinct.

The previous modeling study[20] has presented that thermal conductivities of (1–3)-layer graphene decrease monotonously with the increasing torsion angle because of the slight softening of the acoustic phonon modes caused by the torsion. This monotonous decrease can be regarded as the characteristics of 2D materials. For the classical quasi-2D material, the 10-layer graphene adopted in this work, it can be speculated that several other effects are involved besides the softening of the acoustic phonon modes. Based on the relaxation time approximation, the thermal conductivity can be calculated as

$$\lambda = \sum_{s} \sum_{\text{freq}} c_{\text{ph}} v_{g,\beta}^2 \tau, \tag{10}$$

where c_{ph} is the phonon specific heat and s denotes the phonon branches. In fact, in the classical limit, phonon specific heat is volumetric specific heat for every phonon with particular frequency. In classic MD systems, all phonons are supposed to be excited, and thus, $c_{\text{ph}} = k_B/V$. Detailed information about phonon specific heat can be found in Ref. 43. In the physical view, the torsion changes the lattice structure of MLG so that the phonon spectrum is affected. Since the flexure modes (ZA/ZO modes) of the phonon in quasi-2D structures are quite different from those in 2D membrane materials, the torsion effects on MLG remain unclear, which may be dependent on the changing layer number. Besides, unlike the characteristics of pure 2D materials, the phonon specific heat cannot be constant when the torsion is applied. Thus, the lattice structure of the twisted MLG should be studied first to offer a better understanding of the torsion effects.

B. Lattice structure

In an ideal MLG structure, each layer is formed by hexagonally arranged carbon atoms connected by sp^2 bonds. Since the bonding strength of interlayer couplings is far weaker than that of in-plane atomic bonds, it is reasonable that the torsion changes interlayer structures more remarkably, and its effects on intralayer structures should be slight. To reveal the characteristics of the torsion, the radial distribution functions (RDFs) of carbon atoms in one layer or two different layers of the MLG with $\theta_G = 0°$ are calculated, as shown in Fig. 3. In Fig. 3(a), "Layer 1 to 1"/"Layer 5 to 5" denotes that the central atoms and distribution atoms of RDF are all in Layer 1/Layer 5. In Fig. 3(b), "Layer 1 to 2"/

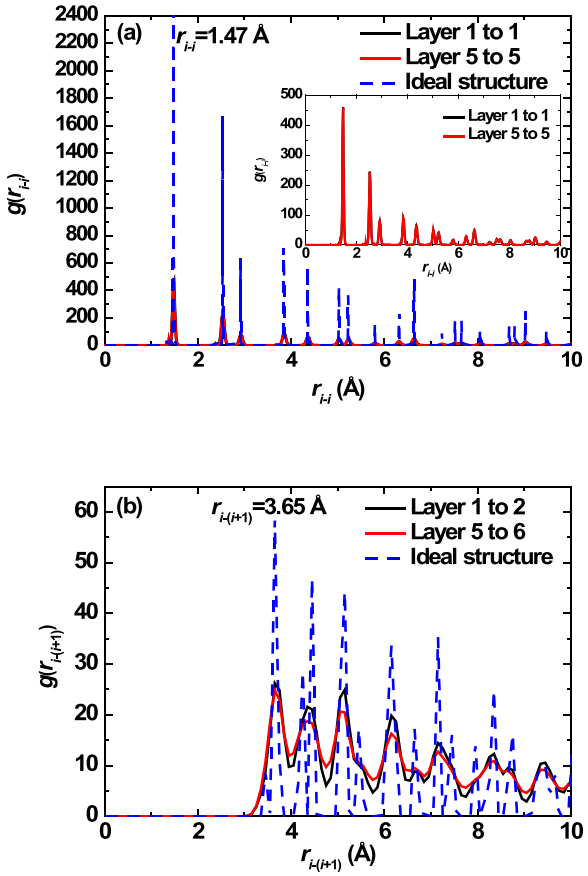

FIG. 3. Radial distribution functions (RDF) of carbon atoms in (a) one layer or (b) two different layers of the MLG with $\theta_G = 0°$.

"Layer 5 to 6" denotes that the central atoms of RDF are in Layer 1/Layer 5, while the distribution atoms are in Layer 2/Layer 6. To reveal the variation in the atomic position, the ideal structure of graphene is defined as the structure of MLG which initially formed in MD simulations without any force or relaxation. The layer with the original location of $z = 1.7$ Å, 5.1 Å, 15.3 Å, and 18.7 Å is defined as Layers 1, 2, 5, and 6. RDF curves with sampling distance d$r = 0.01$ Å for carbon atoms in one layer or two different layers of the MLG with $\theta_G = 0°$ are shown in Fig. 3. The inset figure in Fig. 3(a) shows the same atom distributions between Layer 1 and Layer 5, which reflects the same in-plane lattice structure between the outside layer and the inside layer. The intensity of the RDF peak at $r_{i-I} = 1.47$ Å is stronger because the carbon-carbon bonding length in graphene is 1.47 Å for the ideal structure. However, the out-of-plane atom distribution deviates from the ideal case, as shown in Fig. 3(b). The weak coupling between the layers causes the distinct random distribution whose average interlayer distance is $r_{i-(i+1)} = 3.65$ Å. Besides, distribution between outside layers (the black line) is slightly closer to the ideal case than that between inside layers (the red line) in MLG, due to the more complex interlayer interactions for the inside layers.

Once the torsion is applied to the MLG, interlayer atom distributions for both outside layers and inside layers are changed, as shown in Fig. 4, where the sampling distance is d$r = 0.05$ Å. As the torsion angle θ_G increases from 0° to

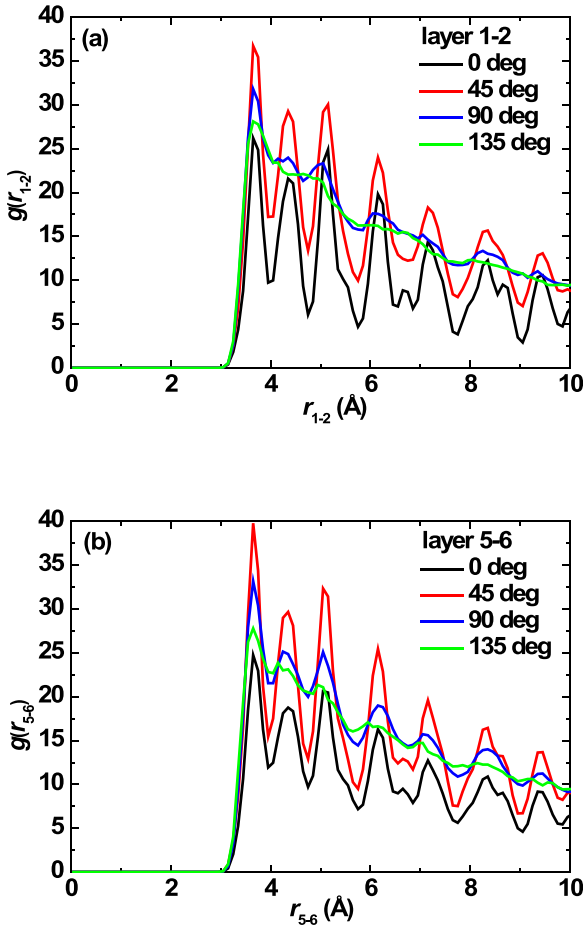

FIG. 4. Radial distribution functions (RDFs) of carbon atoms in (a) Layer 1 and Layer 2 or (b) Layer 5 and Layer 6 for MLG with $\theta_G = 0°$, 45°, 90°, and 135°.

45°, more atom-pairs appear in the range of $0 < r_{i-(i+1)} < 10$ Å so that the RDF curve for $\theta_G = 45°$ is higher than that for $\theta_G = 0°$; meanwhile, more atom pairs appear in the equilibrium distance of $r_{i-(i+1)} = 3.65$ Å. For instance, the value of the first and second peaks for $g(r_{1-2})$ is 26.21 and 21.59 when $\theta_G = 0°$, which is less than the corresponding value of 36.72 and 29.27 when $\theta_G = 45°$. This increase in the RDF indicates that more atoms are clustered in the limit range, which can be regarded as a compression effect. Once θ_G increases to 90°, all the peaks of the RDF curves begin to disappear except for the first peak. For $\theta_G = 135°$, all the peaks except for the first one almost disappear. As is known, the peaks of the RDF curves present the standard distances in the AB-stacking of the graphene layers. The disappearance of peaks indicates the failure of standard AB-stacking, or there exists a lateral dislocation between layers. Figure 4 also presents that the compression effect and dislocation effect occur between both outside layers and inside layers.

To quantify the two effects, the average distances of every nearest atom pair in Layer i and Layer $(i+1)$ ($i = 1$ or 5) at the time just after the relaxation equilibrium, as shown in Fig. 5(a), are calculated. When $\theta_G = 0°$, the distribution is more concentrated in a little range, which is caused by the random lattice vibrations. As the torsion angle increases, as shown in Figs. 5(b) and 5(c), the distribution of the atom pair

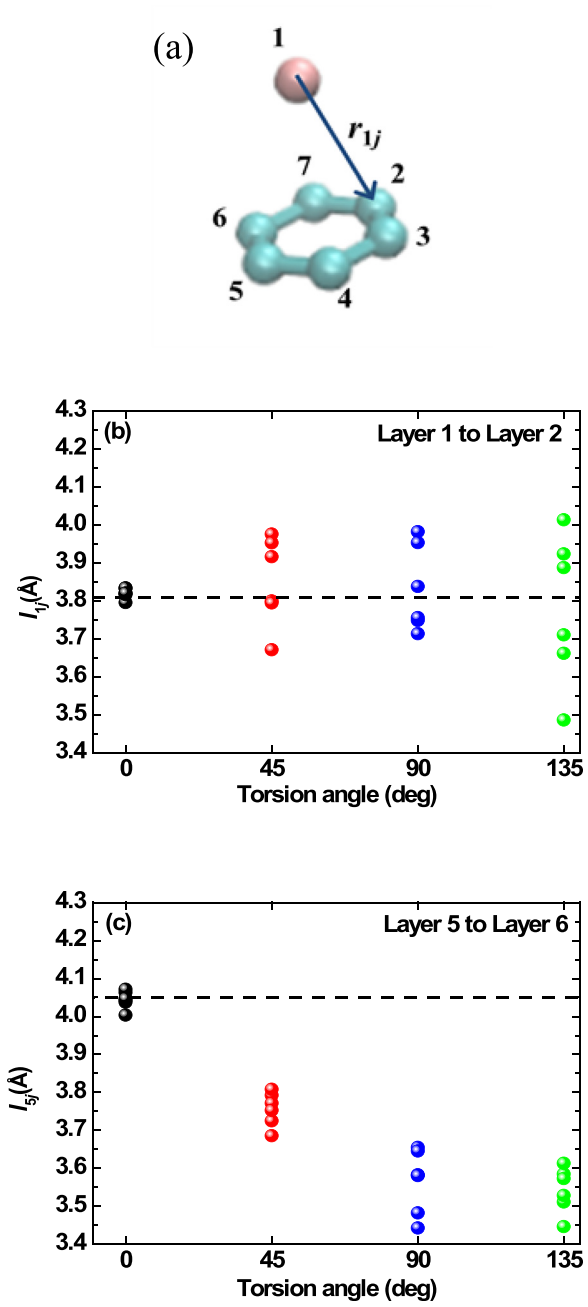

FIG. 5. Schematic diagrams of (a) every nearest atom pair in Layer i and Layer (i + 1), with $i = 1, 2 \ldots 5$, and (b) and (c) the atomic distances of the nearest atom pair in (b) the outside layer and (c) the inside layer for MLG with $\theta_G = 0°$, 45°, 90°, and 135°.

distances presents both the compression effect and the dislocation effect. For the distribution between Layer 1 and Layer 2 [Fig. 5(b)], the range of r_{1j} values becomes larger since the torsion angle θ_G is greater, that is, r_{1j} ranges from 3.796 Å to 3.835 Å for $\theta_G = 0°$, while it ranges from 3.486 Å to 4.014 Å for $\theta_G = 135°$. It is reasonable that the projection of one carbon atom in Layer 1 can just locate at the center of one hexagonally arranged carbon atoms in Layer 2 for an ideal structure of MLG. In this ideal case, all values of r_{1j} should be equal; otherwise, there exists the dislocation for the two layers. Figure 5(b) also indicates that the central value just slightly decreases as the torsion angle increases from 0° to 135°. It can be concluded that the torsion effect leads to large

dislocations and slight compressions for the outside layers. On the other hand, for the inside layers, as shown in Fig. 5(c), the central value decreases apparently from 4.05 Å to 3.55 Å as θ_G increases from 0° to 135°; meanwhile, the range of values becomes larger. It can be concluded that there exist both the compression and the dislocation effects for the inside layers when the torsion is applied.

In fact, there also exists the effect of twisted tension for the twisted MLG. Several previous literature studies have revealed the effect of twist tension on the in-plane thermal conductivity of single-layer graphene.[15,16,19–22] In Wei's work,[15] the size of the twisted graphene is 90×21 Å^2, which has a length-width ratio of 4.286, similar to that of 4.353 in this work. They have twisted the single-layer graphene with angles 180°, 360°, and 480° and found that a twisted angle of 360° will lead to only a decrease of 5% for in-plane thermal conductivity. It can be speculated that the effect of torsion with $\theta_G = 135°$ on the in-plane thermal conductivity of 433.91×99.68 Å^2 graphene can only lead to a drop by about 3%. Thus, the effect of twisted tension can be negligible.

As a result, the torsion effect on the 10-layer graphene can be considered as a complex superposition of the compression effect and the dislocation effect.

C. Phonon dispersion

The phonon dispersion curves, which quantify the relationship between the wave vectors and the frequencies for all the phonon branches in the first Brillouin zone, can be calculated by either the Green function[44,45] or the SED method.[41] In both methods, each equilibrium position of the unit cell should be defined accurately. However, for a twisted MLG as shown in Fig. 1, it is difficult to define the equilibrium position in a regular structure. The positions defined by Eqs. (1)–(4) are the equilibrium position before the relaxation. Once the structure is optimized by the Polak-Ribiere algorithm,[35] unit cells can hardly be described by mathematical regularities. Moreover, the calculation of phonon dispersion for the twisted MLG with 166 740 atoms is almost impossible due to the terrible calculation amount. Wei *et al.*[34] have estimated that the database for a SED calculation of graphene containing 2400 atoms is about 50 Gb. Thus, in this work, an alternative method is used, where the effects of the compression and the dislocation are separately considered, to reveal the torsion effects on the phonon spectrum of MLG. It is assumed that the two effects are uncoupled. The same arithmetic is utilized in Ref. 34, where a flat 10-layer graphene containing 24 000 atoms with the periodic boundary condition is modeled, and the unit cell with 2 atoms is defined. In this work, each layer of MLG can be regarded as a graphene sheet with 2400 atoms, which is used to calculate the SED. Each unit cell contains two carbon atoms.[34] Periodic boundary conductions are utilized in all directions, and the box size in the out-of-plane direction is set as 50 Å, which is large enough. Since the chirality of the MLG is Armchair in the x-direction, the maximum wave vector along ΓM and ΓK should be $2\pi/(3a)$ and $4\pi/(3\sqrt{3}a)$, where $a = 1.47$ Å is the bond length. The wave vector number along ΓM and ΓK is $N_x = N_y = 20$. The timestep of SED calculation is 0.5 fs, and the sampling step number is 10 so that the maximum frequency check[34] can be satisfied. The sampling number of frequency is 1000 to ensure the accuracy of the calculations of phonon lifetime. The compression effect will be studied by adding an extrusion force, while the dislocation effect will be studied by misplacing the interlayer stacking.

1. The dislocation effect

To reveal the dislocation effect, the lateral misplacing is added to the ideal MLG of AB-stacking. Considering the repetitive structure of the graphene plane, the extreme condition of the dislocation is AA-stacking. The phonon dispersion curves of the Γ-M direction for both the AB-stacking and the AA-stacking are calculated by the SED method, as shown in Figs. 6(a) and 6(b). The corresponding branches for the AB-stacking and the AA-stacking locate in almost the same place. It can be evaluated that the dislocation effect on Γ-M phonon dispersion is weak. To quantify the effect, detailed SEDs at $\mathbf{q} = \mathbf{q}_{\Gamma M,max}/2$ are plotted in Fig. 6(c). The positions and the half widths for the corresponding peaks are almost the same, which indicates that the dislocation effects on both the phonon group velocity and lifetime are very weak. Based on Ref. 46, the in-plane thermal conductivity of MLG can be heavily dependent on different interlayer van der Waals bonding strengths. The dislocation changes the interlayer structures of MLG but barely affects the interlayer van der Waals bonding strength because the equilibrium distance remains unchanged. Thus, the dislocation effect on phonon dispersion can be

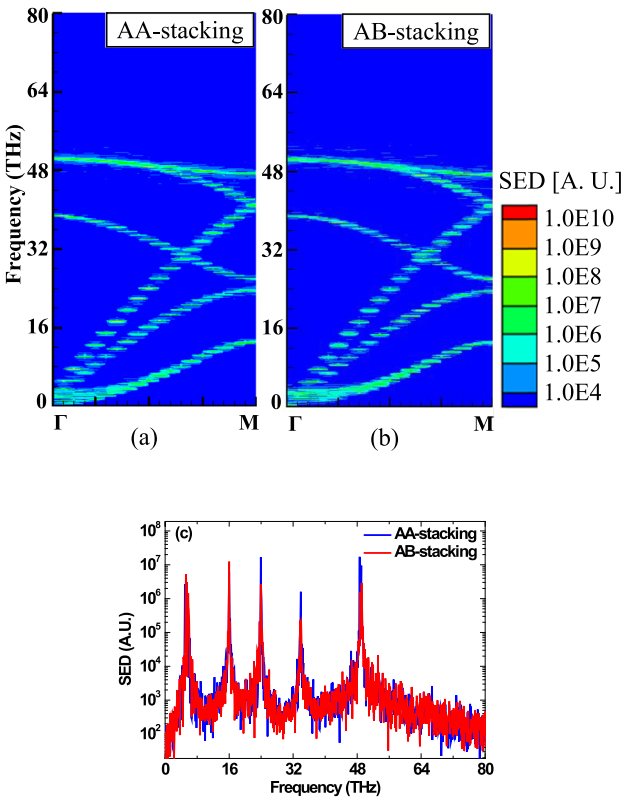

FIG. 6. Phonon dispersions of the Γ-M direction for (a) the AB-stacking and (b) the AA-stacking calculated by the SED method and (c) the detailed SEDs at $\mathbf{q} = \mathbf{q}_{\Gamma M,max}/2$.

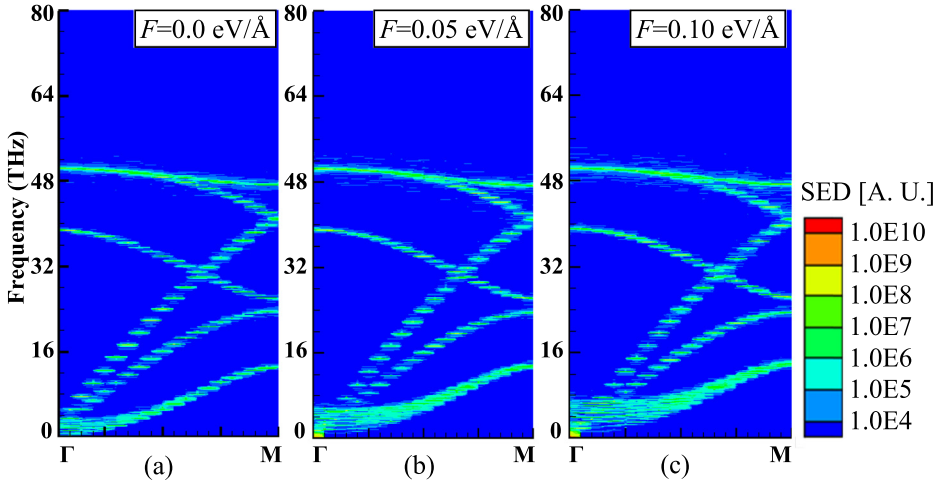

FIG. 7. Phonon dispersions of the Γ-M direction for different compressive forces: (a) $F = 0.0$ eV/Å, (b) $F = 0.05$ eV/Å, and (c) $F = 0.1$ eV/Å.

ignored. Moreover, since the dislocation does not change the volume of the MLG, the phonon specific heat c_{ph} also remains unchanged. In conclusion, the dislocation does not affect the thermal conductivity of the MLG.

2. The compression effect

The same AB-stacking 10-layer graphene as that in Section III C 1 is adopted to reveal the compression effect on phonon dispersion. For the twisted MLG with $\theta_G = 135°$ as shown in Fig. 1(g), the deformation rate is calculated as 86.0%. The two same compressive forces F are applied along the out-of-plane direction on the top and the bottom of the 10-layer graphene to achieve the compression. A series of trials has been carried out to evaluate the value of F, which concludes that the deformation rate of 87.9% for the 10-layer flat graphene is $F = 0.1$ eV/Å. Thus, the compression effect for the twisted MLG with $\theta_G = 135°$ can be equivalent to the compressive forces $F = 0.10$ eV/Å. Similarly, the torsion effect of $\theta_G = 22.5°$ can be equivalent to $F = 0.05$ eV/Å. The relationship of θ_G and F is apparently non-linear because the increase in the compression mainly occurs in the range of $0° < \theta_G < 45°$, as discussed in Section III B.

The phonon dispersion curves of the Γ-M direction for $F = 0$, 0.05, and 0.10 eV/Å are shown in Fig. 7. The compression effect on the ZA branches is noticeable. The width of the ZA branch greatly increases with the increasing F. Since the thermal conductivity is associated with the phonon group velocities and lifetime, it is necessary to quantify the effect of compression on group velocities and lifetime.

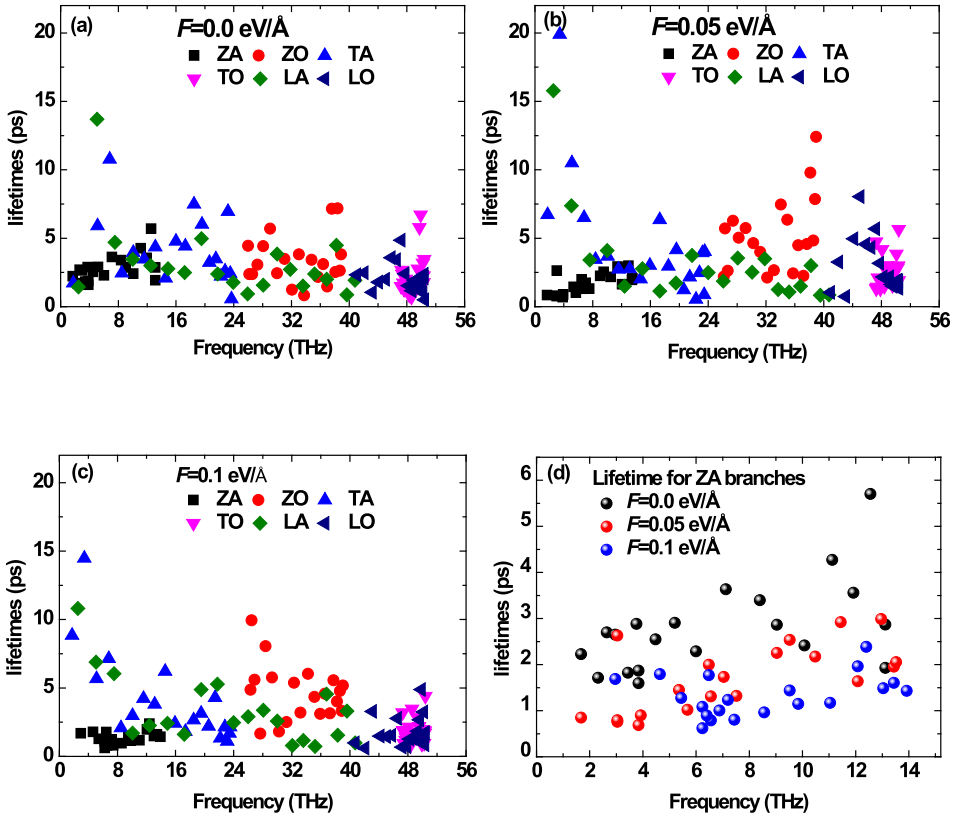

FIG. 8. Phonon lifetimes of all the branches for different compressive forces: (a) $F = 0.0$ eV/Å, (b) $F = 0.05$ eV/Å, and (c) $F = 0.1$ eV/Å. (d) Phonon lifetimes of ZA branches for different compressive forces.

Figures 8(a), 8(b), and 8(c) plot the lifetime for all the branches calculated by Eq. (9). Since the effect of compression on the ZA branches is the most noticeable, the Γ-M lifetimes of ZA branches for $F = 0$, 0.05, and 0.10 eV/Å are displayed in Fig. 8(d). As F increases from 0 to 0.10 eV/Å, the increasing compression effect leads to the decrease in ZA lifetimes. For $0 < F < 0.05$ eV/Å, the effect of compression on lifetimes is more apparent, which can be confirmed by the comparison of black and red dots in Fig. 8(d), whereas for $F > 0.05$ eV/Å, the effect of compression on lifetimes is weak. Figures 8(a), 8(b), and 8(c) also indicate a slight increase for all the optic branches, ZO, TO, and LO branches, with the increase in the compression. The out-of-plane compression causes the phonon scattering of flexure modes and thus decreases the ZA lifetimes. The phonon group velocities can be obtained by the phonon dispersion curves, as $v_{g,x} = \partial\omega/\partial q_x$, which are shown in Fig. 9. The group velocities for all the branches are nearly unchanged, except for the ZA branches. A slight increase in the ZA group velocity is found for $|\mathbf{q}| < |\mathbf{q}_{\Gamma M,\max}|/2$, with the increase in the compression, where $|\mathbf{q}_{\Gamma M,\max}| = 2\pi/3a$, with $a = 1.47$ Å denoting the bond length.

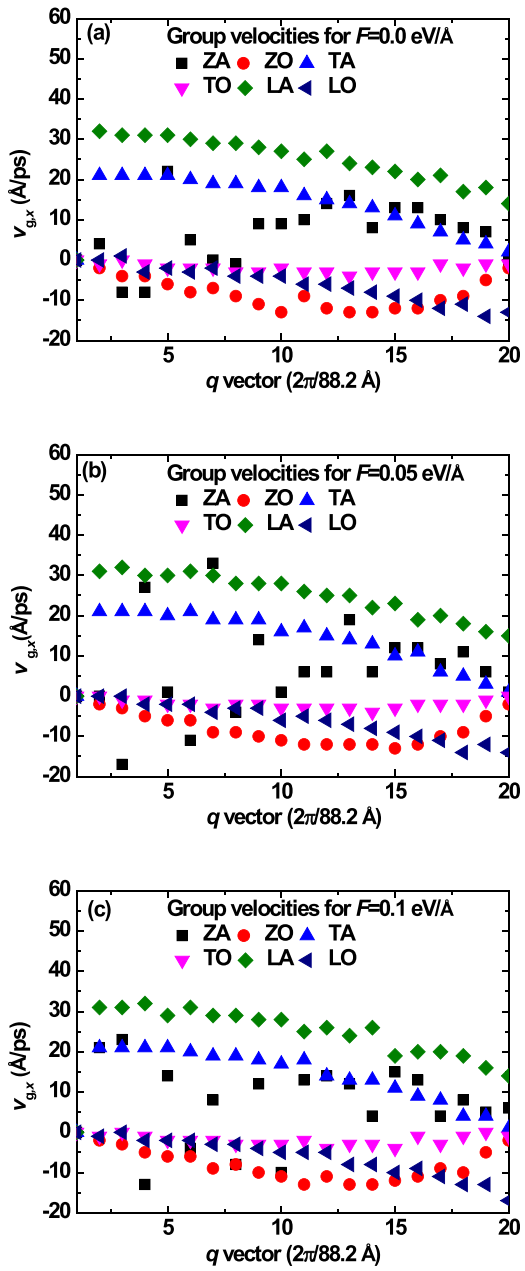

FIG. 9. Phonon group velocities of all the branches for different compressive forces: (a) $F = 0.0$ eV/Å, (b) $F = 0.05$ eV/Å, and (c) $F = 0.1$ eV/Å.

TABLE II. Deformation rates, phonon heat capacities, phonon property terms, and thermal conductivities for different compressive forces.

Compressive force F (eV Å^{-1})	0.0	0.05	0.1
Corresponding torsion angle θ_G	0°	22.5°	135°
Deformation rate	100%	92.9%	87.9%
Phonon specific heat c_{ph} (J K^{-1} m^{-3})	C	1.076C	1.138C
Phonon property term $v_{g,\beta}^2\tau$ (10^{-3} m^2 s^{-1})	8.46	7.77	7.65
Thermal conductivity (10^{-3} W m^{-1} K^{-1})	8.46C	8.36C	8.71C

Since all phonons are supposed to be excited, the phonon specific heat can be calculated by $c_{ph} = k_B/V$. It can be defined that $c_{ph} = C$ when $F = 0.0$ eV/Å. Thus, the phonon specific heat can be calculated based on the deformation rates, as shown in Table II. As the compression force increases, the specific heat also increases due to the decrease in the material volume. In fact, as a kind of quasi-2D material, it is reasonable that the phonon specific heat cannot be constant.

As a result, the compression effect decreases the phonon lifetimes of ZA branches and increases the ZA group velocities and the phonon specific heat. Thus, the evolution curve of the thermal conductivities shown in Fig. 2(b) presents the complex shape. To quantify the compression effect, the phonon property term $v_{g,\beta}^2\tau$ and the thermal conductivity calculated by Eq. (10) are presented in Table II. The phonon property term decreases more significantly from 8.46×10^{-3} m^2 s^{-1} to 7.77×10^{-3} m^2 s^{-1} for $0° < \theta_G < 22.5°$, while it decreases slightly from 7.77×10^{-3} m^2 s^{-1} to 7.65×10^{-3} m^2 s^{-1} for $22.5° < \theta_G < 135°$. It can be speculated that the decrease in the phonon lifetimes caused by the compression effect is the dominant factor when the torsion angle is small. Once the torsion angle becomes larger, the increase in the phonon specific heat leads to the increase in thermal conductivity since the effect of the phonon property term becomes weaker and weaker. The thermal conductivity calculated by Eq. (10) first decreases from 8.46 C to 8.36 C for $0° < \theta_G < 22.5°$ and then increases from 8.36 C to 8.71 C. Thus, the valley of the thermal conductivity evolution presented in Fig. 2(b) can be explained by the compression effect.

IV. CONCLUSIONS

This work utilizes the EMD method to study the effects of torsion on the thermal conductivities of 10-layer graphene. The radial distribution functions are calculated to reveal the lattice structures of the twisted MLG. The SED method is adopted to reveal the phonon dispersion. The conclusions are as follows:

(1) The high thermal conductivity of 5080 W m^{-1} K^{-1} is obtained for pure 10-layer graphene with an in-plane size of 433.91 × 99.68 Å^2. The thermal conductivity of

the twisted 10-layer graphene decreases slightly first and then increases with the increasing torsion angle, and the valley is located at $\theta_G = 22.5°$ with the lowest thermal conductivity of 4692.40 W m^{-1} K^{-1}.

(2) As the torsion angle θ_G increases from 0° to 45°, more atom pairs appear in the equilibrium distance of $r_{i-(i+1)} = 3.65$ Å, and the RDF curves are raised up, which indicate the torsion effect on the lattice structure. As θ_G increases to 90°, all the peaks of the RDF curves begin to disappear except for the first peak. For $\theta_G = 135°$, all the peaks except for the first one almost disappear. Based on the RDF curves, the torsion effect on the 10-layer graphene can be considered as a complex superposition of the compression effect and the dislocation effect.

(3) The phonon dispersion calculated by the SED method indicates the compression effect and the dislocation effect on the thermal conductivity. The dislocation effect on phonon dispersion can be ignored. The compression effect decreases the phonon lifetimes of ZA branches and increases the ZA group velocities as well as the phonon specific heat. The decrease in the phonon lifetimes caused by the compression effect is the dominant factor for $0° < \theta_G < 22.5°$. Once the torsion angle becomes larger, as $22.5° < \theta_G < 135°$, the increase in the phonon specific heat leads to the increase in thermal conductivity, which becomes more dominant since the effect of the phonon property term becomes weaker and weaker.

ACKNOWLEDGMENTS

This study was partially supported by the National Science Fund for Distinguished Young Scholars of China (No. 51525602), the National Science Fund of China (No. 51606064), and the Fundamental Research Funds for the Central Universities (No. JB2016133).

[1]A. A. Balandin, S. Ghosh, W. Bao, I. Calizo, D. Teweldebrhan, F. Miao, and C. N. Lau, Nano Lett. **8**, 902 (2008).
[2]L. A. Jauregui, Y. Yue, A. N. Sidorov, J. Hu, Q. Yu, G. Lopez, R. Jalilian, D. K. Benjamin, D. A. Delk, W. Wu, Z. Liu, X. Wang, Z. Jiang, X. Ruan, J. Bao, S. S. Pei, and Y. P. Chen, ECS Trans. **28**, 73 (2010).
[3]L. Lindsay, D. A. Broido, and N. Mingo, Phys. Rev. B **82**, 115427 (2010).
[4]K. Saito, J. Nakamura, and A. Natori, Phys. Rev. B **76**, 115409 (2007).
[5]W. J. Evans, L. Hu, and P. Keblinski, Appl. Phys. Lett. **96**, 203112 (2010).
[6]J. N. Hu, S. Schiffli, A. Vallabhaneni, X. L. Ruan, and Y. P. Chen, Appl. Phys. Lett. **97**, 133107 (2010).
[7]E. Pop, V. Varshney, and A. K. Roy, Mater. Res. Bull. **37**, 1273 (2012).
[8]Y. Xu, Z. Y. Li, and W. H. Duan, Small **10**, 2182 (2014).
[9]E. McCann and V. I. Fal'ko, Phys. Rev. Lett. **96**, 086805 (2006).
[10]G. Liu, W. Jin, and N. Xu, Chem. Soc. Rev. **44**, 5016 (2015).
[11]S. Mohammadi, H. Shariatpanahi, F. A. Taromi, and J. Neshati, Mater. Res. Bull. **80**, 7 (2016).
[12]E. M. Wouterson, "Unusual nano-scale phenomena in highly porous polymer systems containing graphite nano-sheets," in Program & Abstracts of the International Symposium on Engineering Plastics (2011).
[13]C. Si, X. D. Wang, Z. Fan, Z. H. Feng, and B. Y. Cao, Int. J. Heat Mass Transfer **107**, 450 (2017).
[14]Y. Kuang, L. Lindsay, and B. Huang, Nano Lett. **15**, 6121 (2015).
[15]N. Wei, L. Xu, H. Q. Wang, and J. C. Zhang, Nanotechnology **22**, 105705 (2011).
[16]X. Li, K. Maute, M. L. Dunn, and R. Yang, Phys. Rev. B **81**, 245318 (2010).
[17]Z. Wei, J. Yang, W. Chen, K. Bi, D. Li, and Y. Chen, Appl. Phys. Lett. **104**, 081903 (2014).
[18]S. Ghosh, W. Bao, D. L. Nika, S. Subrina, E. P. Pokatilov, C. N. Lau, and A. A. Balandin, Nat. Mater. **9**, 555 (2010).
[19]C. X. Yu and G. Zhang, J. Appl. Phys. **113**, 044306 (2013).
[20]R. Chellattoan and S. P. Sathian, Solid State Commun. **173**, 1 (2013).
[21]H. Shen, Mol. Phys. **112**, 2614 (2014).
[22]X. Wei, G. Guo, T. Ouyang, and H. Xiao, J. Appl. Phys. **115**, 154313 (2014).
[23]B. Y. Cao, W. J. Yao, and Z. Q. Ye, Carbon **96**, 711 (2016).
[24]W. Cai, A. L. Moore, Y. Zhu, X. Li, S. Chen, L. Shi, and R. S. Ruoff, Nano Lett. **10**, 1645 (2010).
[25]Y. H. Zhao, Z. K. Wu, and S. H. Bai, Int. J. Heat Mass Transfer **101**, 470 (2016).
[26]H. D. Wang, K. Kurata, T. Fukunaga, H. Ago, H. Takamatsu, X. Zhang, T. Ikuta, K. Takahashi, T. Nishiyama, and Y. Takata, J. Appl. Phys. **119**, 244306 (2016).
[27]D. L. Nika, E. P. Pokatilov, A. S. Askerov, and A. A. Balandin, Phys. Rev. B **79**, 155413 (2009).
[28]J. H. Seol, I. Jo, A. L. Moore, L. Lindsay, Z. H. Aitken, M. T. Pettes, X. Li, Z. Yao, R. Huang, D. Broido, N. Mingo, R. S. Ruoff, and L. Shi, Science **328**, 213 (2010).
[29]Z. Aksamija and I. Knezevic, Appl. Phys. Lett. **98**, 141919 (2011).
[30]Y. Xu, X. B. Chen, and J. S. Wang, Phys. Rev. B **81**, 195425 (2010).
[31]Z. Huang, T. S. Fisher, and J. Y. Murthy, J. Appl. Phys. **108**, 094319 (2010).
[32]N. Yang, X. Ni, J. W. Jiang, and B. Li, Appl. Phys. Lett. **100**, 093107 (2012).
[33]J. R. Lukes and H. L. Zhong, J. Heat Trans. - Trans. ASME **129**, 705 (2007).
[34]Z. Wei, J. Yuan, K. Bi, and Y. Chen, J. Appl. Phys. **116**, 153503 (2014).
[35]E. Polak, *Optimization: Algorithms and Consistent Approximations* (Springer, New York, 1997).
[36]L. Lindsay and D. A. Broido, Phys. Rev. B **81**, 205441 (2010).
[37]S. Plimpton, J. Comput. Phys. **117**, 1 (1995).
[38]R. Kubo, Rep. Prog. Phys. **29**, 255 (1966).
[39]J. Li, L. Porter, and S. Yip, J. Nucl. Mater. **255**, 139 (1998).
[40]H. Zhang, G. Lee, and K. Cho, Phys. Rev. B **84**, 115460 (2011).
[41]J. A. Thomas, J. E. Turney, R. M. Iutzi, C. H. Amon, and A. J. H. McGaughey, Phys. Rev. B **81**, 081411 (2010).
[42]A. Henry and G. Chen, Phys. Rev. B **79**, 144305 (2009).
[43]J. E. Turney, E. S. Landry, A. J. H. McGaughey, and C. H. Amon, Phys. Rev. B **79**, 064301 (2009).
[44]C. Campañá and M. H. Müser, Phys. Rev. B **74**, 075420 (2006).
[45]L. T. Kong, Comput. Phys. Commun. **182**, 2201 (2011).
[46]Z. Wei, Y. Chen, and C. Dames, Appl. Phys. Lett. **102**, 011901 (2013).